IOP Publishing Nanotechnology
Nanotechnology **25** (2014) 094008 (11pp) doi:10.1088/0957-4484/25/9/094008

Nanocrystalline cellulose applied simultaneously as the gate dielectric and the substrate in flexible field effect transistors

D Gaspar, S N Fernandes, A G de Oliveira, J G Fernandes, P Grey, R V Pontes, L Pereira, R Martins, M H Godinho and E Fortunato

CENIMAT/I3N, Departamento de Ciência dos Materiais, Faculdade de Ciências e Tecnologia, Universidade Nova de Lisboa, Campus de Caparica, 2829-516 Caparica, Portugal

E-mail: rm@uninova.pt, mhg@fct.unl.pt and emf@fct.unl.pt

Received 2 August 2013, revised 10 October 2013
Published 12 February 2014

Abstract

Cotton-based nanocrystalline cellulose (NCC), also known as nanopaper, one of the major sources of renewable materials, is a promising substrate and component for producing low cost fully recyclable flexible paper electronic devices and systems due to its properties (lightweight, stiffness, non-toxicity, transparency, low thermal expansion, gas impermeability and improved mechanical properties).

Here, we have demonstrated for the first time a thin transparent nanopaper-based field effect transistor (FET) where NCC is simultaneously used as the substrate and as the gate dielectric layer in an 'interstrate' structure, since the device is built on both sides of the NCC films; while the active channel layer is based on oxide amorphous semiconductors, the gate electrode is based on a transparent conductive oxide.

Such hybrid FETs present excellent operating characteristics such as high channel saturation mobility (>7 cm^2 V^{-1} s^{-1}), drain–source current on/off modulation ratio higher than 10^5, enhancement n-type operation and subthreshold gate voltage swing of 2.11 V/decade. The NCC film FET characteristics have been measured in air ambient conditions and present good stability, after two weeks of being processed, without any type of encapsulation or passivation layer. The results obtained are comparable to ones produced for conventional cellulose paper, marking this out as a promising approach for attaining high-performance disposable electronics such as paper displays, smart labels, smart packaging, RFID (radio-frequency identification) and point-of-care systems for self-analysis in bioscience applications, among others.

Keywords: nanopaper, paper electronics, paper transistor, nanocellulose

(Some figures may appear in colour only in the online journal)

1. Introduction

Today's electronics are manufactured with expensive materials associated with polluting technologies and without the possibility of being recyclable. On the other hand, cellulose paper is one of the most common and cheapest of all substrate materials used in our society, and is recyclable and biocompatible; however its application window is currently limited to being a carrier of printed information and packaging. Cellulose is the Earth's major biopolymer and of tremendous global economic importance, especially in Europe, representing 30% of the world's total production. Nevertheless the use of paper

 © 2014 IOP Publishing Ltd Printed in the UK

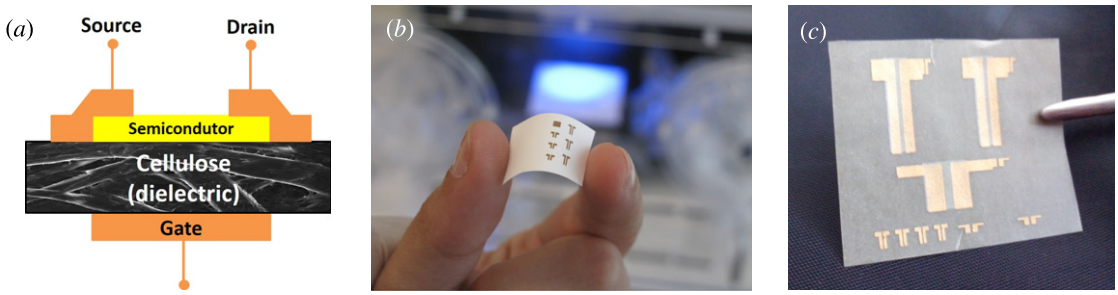

Figure 1. Representation of electronic devices developed at FCT-UNL where the cellulose paper is simultaneously the gate dielectric material and the substrate; (a) the first field effect transistor using metal oxide as the semiconductor [2], (b) a photograph and (c) the CMOS using n-type and p-type metal oxide semiconductors [4].

could be expanded tremendously if electronic, sensor and display applications could also be applied on it and through it. Some promising applications have already been demonstrated, like solar cells, displays, capacitors, actuators, gas sensors, magnetic devices and batteries, but in all of these applications paper has a passive function since it is used as a substrate, not taking an active role in the device's working principle [1]. In this paper and following our previous work [2–7], we use a membrane of nanocrystalline cellulose (NCC), also known as nanopaper, simultaneously as the dielectric layer of a field effect transistor (FET) and as the substrate. In this new approach we are using nanocrystalline cellulose as an 'interstrate' structure, since the device is built on both sides of the nanocrystalline cellulose membrane, similar to the structure presented in figure 1(a), reducing the production steps by avoiding the deposition of the gate dielectric.

Another salient feature of cellulosic films is the formation of liquid crystalline networks, which can couple between orientational order and mechanical strain. In these cellulosic-based materials the change of the orientational order was attained by the presence of moisture, and a motor, that can extract mechanical work from a difference in humidity, was built [8]. Moreover these low cost iridescent materials with added NCC particles can show optical features similar to those that can be found in *Papaver rhoeas* petals, which can lead to the improvement of new materials for application in, for example, tunable soft reflective screens and devices. In addition, natural films of this type can be used as soft templates for generating other materials with biomimetic structures [9].

In the past few years, research on cellulose has increased intensively, especially as regards the form of new nanostructured materials, like nanocrystalline cellulose [10–12], microfibrillar/nanofibrillar cellulose [13] and bacterial cellulose [14]. Cellulose alone is limited to its functionalities, but the three-dimensional hierarchical structures that compose cellulose fibers at different scales open up new opportunities for new fields, ranging from electrical to medical applications [15–17].

Among all these cellulose nanostructures, nanocrystalline cellulose has attracted particularly broad attention mainly due to its properties, like light weight, stiffness, non-toxicity, transparency, low thermal expansion, gas impermeability and improved mechanical properties [18–20]. This nanostructured material can also replace some petrochemical-based products and is cheaper than the majority of other kinds of high-performance nanostructured materials, being one of the major sources of renewable materials, and improving also the environmental footprint. In table 1 we present some of the main applications of nanocrystalline cellulose [16].

Cotton fiber is the purest source of cellulose, is the most significant natural fiber, and is unique in many ways. It presents a higher content of cellulose among the plant cells, with mostly 88–96% α-cellulose. The non-cellulosic products are found on the outer layer or inside the lumens of the fibers. However, its secondary cell wall is 100% cellulose, which gives access to pure cellulose relatively easily once the very thin primary cell wall is removed. However, the specific chemical compositions of cotton vary according to the varieties, growing environments (soil, water, temperature, pests, etc) and maturity. Cotton cellulose also has the longest molecular chain lengths as well as the most crystalline structure. Hence, cotton is an example of a cellulose structure with utmost order [21–23].

In this paper we report for the first time the use of cotton-based nanocrystalline cellulose membranes simultaneously as the substrate and the gate dielectric in metal oxide field effect transistors, fully processed at room temperature [24–27].

2. Experimental details

In the following we explain the experimental procedure followed to obtain the NCC used in this study.

2.1. Nanocrystalline cellulose film preparation

Nanocrystalline cellulose rods were obtained from microcrystalline particles produced from cotton, described as follows (see the scheme in figure 2).

Microcrystalline cellulose (MCC) particles derived from hydrophilic cotton wool (Hassemed, 100% cotton) were obtained by hydrochloric acid (37%, p.a., Panreac) hydrolysis as described in the literature [28–30] with some minor adaptations (see figure 2(b1)). Typically 5 g of cotton wool was hydrolyzed with 2.5N hydrochloric acid (HCl, p.a., Panreac) at 85 °C for 3 h under reflux. The hydrolyzed MCC particles were neutralized with distilled water until a neutral pH was reached, and further washed through filtration with water and acetone. The particles were allowed to dry in a chamber with controlled

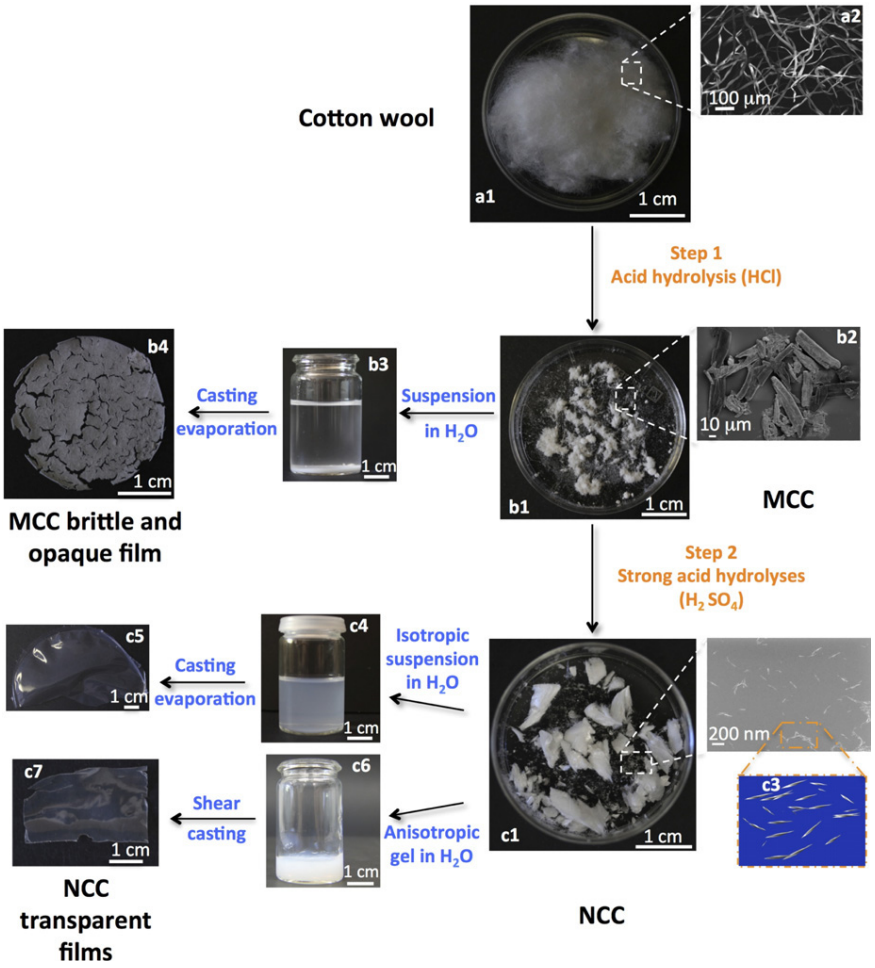

Figure 2. Schematic representation of the different paths involved in the NCC synthesis and film preparation. Picture images of: (a1) cotton, the raw material; (b1) MCCs, obtained by HCl hydrolysis; (c1) freeze-dried NCCs, obtained by H_2SO_4 hydrolysis; (b3), (c4) and (c6) show film precursor suspensions and (b4), (c5) and (c7) show MCC and NCC solid films, respectively; (a2) cotton fibers, (b2) MCC and (c2) NCC are SEM pictures; (c3) is a schematic 3D drawing of twisted NCC particles.

Table 1. Applications of nanocrystalline cellulose.

Nanocrystalline cellulose applications	Products
Electronic/optoelectronic (as the substrate and as a proposed component)	Displays
	Sensors
	Solar cells
	Intelligent windows
	Memories, batteries
Food	Flavor carriers
	Suspension stabilizers
	Thickener
Packaging	Improved oxygen impermeability
Paper	Enhancement of the fiber–fiber bond strength
	Barrier in greaseproof-type papers
	Improvements of mechanical properties
Medical	Antimicrobial films
	Intestinal disorders
	Water absorbent pads
Pharmaceutical/cosmetics	Excipients
	Biocoatings

humidity (∼10%) until constant weight was obtained (∼85% yield).

The dimensions of the MCC are in the ranges of 160–12 μm length and 25–2 μm diameter and were obtained from the scanning electron microscopy (SEM) images of the particles. The lengths and diameter of individual microparticles/nanoparticles visible in these images were measured with ImageJ (version 1.45s, http://imagej.nih.gov/ij/) and scaled according to the magnification quoted by the microscope software. A minimum of 50 length measurements were taken for each sample.

Nanocrystalline cellulose particles were prepared on the basis of the methods of Gray *et al* [11, 31] and Orts *et al* [32] with minor adaptations (see figure 2(c1)). Microcrystalline cellulose was hydrolyzed with sulfuric acid (97%, p.a., Merck) with an acid/solid ratio of 17.5 at 45 °C for 130 min under vigorous stirring. The resultant suspension was washed with ultrapure water by successive dilution and centrifugation (at 1200 rpm for 20 min) until the supernatant was turbid (that occurs at approximately pH 1.9–3.8). The resulting suspension was placed in a Spectra/Por 4 cellulose membrane (Spectrum) and dialyzed against ultrapure water until a pH of 6–7 was reached. A suspension of 0.5–0.7% of NCC, determined by gravimetry, was obtained. The content of NCC in the suspension was increased by subsequent centrifugations (at 14 500 rpm for 20 min) and a gel-type substance was obtained. The water used in these experiments was purified by using a Millipore Elix Advantage 3 purification system.

Solid films of microcrystalline cellulose were prepared by slow casting and evaporation of water from suspensions of 1–5% MCC under ambient conditions in polystyrene Petri dishes (90 mm diameter). The resulting films had a thickness of approximately 60 μm, estimated from the average of ten measurements made using a Mitutoyo digital micrometer; however they are too brittle to undergo further treatment (figure 2(b4)).

Free-standing transparent NCC films were prepared by two different methods: solvent casting and evaporation, further designated only as evaporation (NCC E), and sheared casting, further designated only as casting (NCC C). Solid films of the nanocrystalline cellulose were prepared by slow casting and evaporation of water from 60 ml (0.3–0.7% NCC content; figure 2(c4)) of the NCC suspension under ambient conditions in polystyrene Petri dishes (90 mm diameter). The resulting films had a thickness of approximately 30–55 μm (figure 2(c5)).

Films were also prepared from suspensions with 5–6% NCC content (figure 2(c6)), cast, and sheared simultaneously by moving a calibrated Gardner knife from Braive Instruments at 1.25 mm s^{-1} over a polystyrene sheet. The films, 35–55 μm thick, were allowed to dry at room temperature (see figure 2(c7)).

2.2. Film characterization

Scanning electron microscopy (SEM) images of the nanocrystalline cellulose films were acquired with a Carl Zeiss Auriga crossbeam (SEM-FIB) workstation instrument equipped with an Oxford energy dispersive x-ray spectrometer. The SEM images were taken in the in-lens mode with an acceleration voltage of 2 kV and aperture size of 30 μm. The nanocrystalline cellulose films were glued on aluminum stubs using a double-sided carbon tape and coated with a thin carbon layer (< 20 nm) using a Q300T D Quorum sputter coater.

The structural analysis of the samples was done via x-ray diffraction (XRD, PANalytical, model X'Pert Pro) in Bragg–Brentano geometry with Cu Kα line radiation (λ = 1.5406 Å) at 45 kV and 40 mA, the instrument being equipped with an X'Celerator detector. The XRD patterns were collected with a scanning step of 0.0334° over the angular 2θ range 10°–40°, with a total acquisition time of 4 min.

The crystallinity index (I_c) was determined using the empirical method proposed by Segal *et al* [33]:

$$I_c = \frac{I_{(002)} - I_{(am)}}{I_{(002)}} \times 100 \quad (1)$$

where $I_{(002)}$ is the maximum intensity of diffraction of the (002) lattice peak at a 2θ angle between 21° and 23°, which represents the crystalline counterpart. $I_{(am)}$ is the intensity of diffraction of the amorphous material, which is taken at a 2θ angle between 18° and 20° where the intensity is at a minimum. It should be noted that the crystallinity index is only valid as a comparison basis, as it is used to indicate the order of crystallinity rather than the crystallinity of crystalline regions.

The crystallite size was inferred through the Scherrer equation [34]:

$$D_{hkl} = \frac{0.9\lambda}{\beta \cos\theta} \quad (2)$$

where D_{hkl} is the crystallite size in the direction normal to the hkl lattice planes, λ is the x-ray radiation wavelength, β is the full width at half-maximum (FWHM) of the diffraction peak and θ is the corresponding Bragg angle.

The diffractograms obtained were analyzed with specific software (HighScore Plus) that allows the deconvolution of $K\alpha_1$ and $K\alpha_2$ cases. The data obtained from the XRD measurement are treated to obtain more accurate information on peak parameters such as position, intensity, width and shape. Using the software, the background is determined, the peaks are searched ($K\alpha_1$ and $K\alpha_2$ not separated) and it is possible to fit the profile of the peaks, in which $K\alpha_1$ and $K\alpha_2$ are deconvoluted. The peak profile characteristics are calculated by applying adjustable, mathematical profile functions. The software also calculates the FWHM.

Thermogravimetric analysis measurements (TGA) were carried out with a simultaneous thermal analyzer (TGA-DSC-STA 449 F3 Jupiter). Approximately 3 mg of each sample was loaded into an aluminum pan and heated from 25 to 550 °C with a heating rate of 5 °C min^{-1}. All the measurements were performed under air atmosphere.

Fourier transform infra-red (FTIR) spectroscopy data were recorded using an attenuated total reflectance (ATR) sampling accessory (Smart iTR) equipped with a single-bounce diamond crystal on a Thermo Nicolet 6700 spectrometer. The

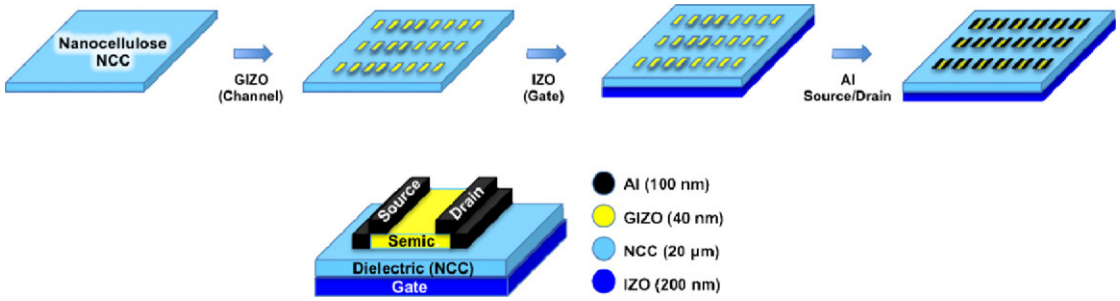

Figure 3. Schematics of the process of fabrication of FETs using NCC as the gate dielectric, and the corresponding staggered-bottom gate structure used in this work.

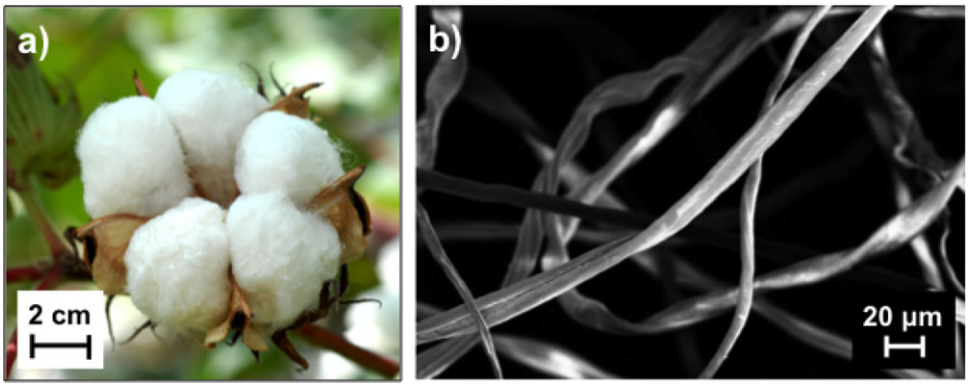

Figure 4. Natural cotton (a) bolls and (b) cellulose fibers.

spectra were acquired under the following conditions: incident angle of 45°; 4000–650 cm^{-1} range; 4 cm^{-1} resolution; 32 scans; 20 °C.

The optical transmittance measurements were performed with a Shimadzu UV/visible 3100 PC double-beam spectrophotometer in the wavelength range from 200 to 2500 nm, with a scan of 2 nm and using air as the reference.

Photographs of the microcrystalline/nanocrystalline cellulosic suspensions and membranes were taken with a Casio EX-F1 Exilim Pro and a Canon EOS 550D photo camera. The software blender, version 2.57b, was used to obtain the 3D drawing of the nanocrystalline cellulose particles.

2.3. Field effect transistor fabrication and characterization

The devices were produced using the two different transparent and flexible nanocrystalline cellulose membranes in a staggered-bottom gate FET structure, acting as the gate dielectric, without any kind of surface treatment.

On one side of the nanocrystalline cellulose membrane a 40 nm thick GIZO (Ga_2O_3–In_2O_3–ZnO; 1:2:2 mol%) layer (the active oxide semiconductor) was deposited by r.f. magnetron sputtering, at room temperature, in an AJA ORION system, following the procedures described elsewhere [22].

The aluminum source and drain contacts were deposited afterwards by e-beam evaporation (100 nm) over the patterned semiconductor region. The semiconductor channel and the source and drain were patterned with shadow masks with a channel width (W) of 2220 μm and length (L) of 210 μm ($W/L = 10.6$). The devices were measured at atmospheric pressure at a temperature of 23 °C and relative humidity of 40%. On the opposite side of the nanocrystalline cellulose membrane an IZO (In_2O_3–ZnO; 5:2 mol%) film (200 nm) was deposited by r.f. sputtering at room temperature, serving as the gate electrode [35].

The FETs were subjected to annealing in air for 30 min at 150 °C at atmospheric pressure.

The FETs were electrically analyzed in the dark at RT using a Cascade Microtech M150 microprobe station connected to a semiconductor parameter analyzer (Agilent 4155C) controlled by the software Metrics ICS. The films' electrical capacitance (C) was determined with impedance spectroscopy (IS; Gamry Instruments Reference 600 Potentiostat) using a parallel plate configuration. Figure 3 shows a schematic representation of the proposed device configuration including all the fabrication steps as well as the different layers and corresponding thickness.

3. Results and discussion

3.1. Cotton fibers and nanocrystalline cellulose membranes

The raw cotton fibers have been observed by SEM in order to investigate the surface morphology, and a flat twisted ribbon form (figure 4(b)) characteristic of the dried fibers [21] was revealed. The average width obtained was 10–15 μm, which is in good accordance with reports found in the literature [36]. This twisted ribbon shape associated with the flatness of

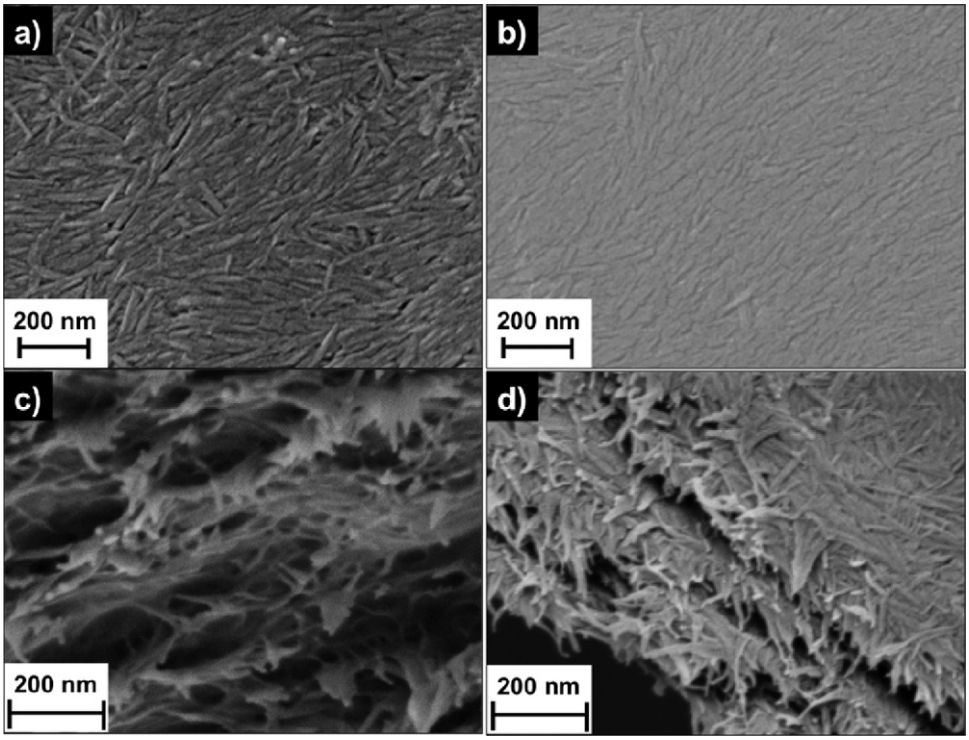

Figure 5. SEM micrographs of the two nanocrystalline cellulose membranes: (a) surface morphology for NCC obtained by casting, (b) surface morphology for NCC obtained by evaporation, and the corresponding cross sections: (c) and (d) respectively.

the fibers increases its surface area and favors chemical reactions such as acid hydrolysis by promoting the cleavage and extraction of the amorphous regions [37].

Figure 5 shows the SEM micrographs of the two nanocrystalline cellulose membranes. From the images we can see that nanocrystalline cellulose film prepared by shear casting presents a smooth structure but one that is less compact than the one prepared by evaporation, which is corroborated by the corresponding cross sections in figures 5(c) and (d). A needle-like structure is observed in both samples, with nanocrystalline cellulose particles showing average dimensions, measured from SEM images, of ∼188 nm length by ∼19 nm thickness, with an average aspect ratio of ∼10; these values are in good agreement with the ones presented by Elazzouzi-Hafraoui *et al* [38].

Due to the different film preparation methods, shear casting or slow casting and evaporation, from two different solutions, anisotropic gel and isotropic suspension, the film surface and cross section show distinct morphologies. Despite the use of an anisotropic NCC suspension, the shear seems to induce a more open membrane structure, as shown in figure 5(c), compared with the membrane obtained by slow evaporation from an isotropic solution. The usual chiral nematic arrangement obtained for NCC films [39] seems to be disrupted by the shear for the sample prepared from the gel. An improved homogeneous cross section is obtained for the films prepared by evaporation.

In order to analyze the crystallinity as well as the crystallite size of the two nanocrystalline cellulose membranes, x-ray diffractometry was carried out. The results are shown in figure 6, in comparison with those for the cotton fibers, the

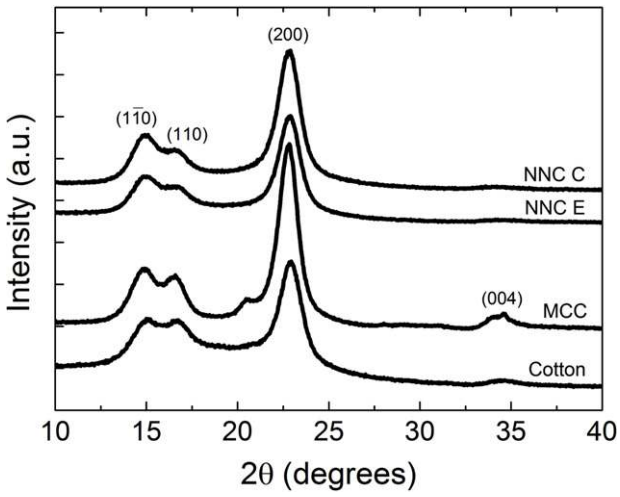

Figure 6. XRD diffractograms for the unmodified cotton fibers, microcrystalline cellulose (MCC) and two kinds of nanocrystalline cellulose membranes (NCC E and NCC C).

intermediate product MCC and the two nanocrystalline cellulose films. From the data it is possible to qualitatively evaluate that all samples present the same diffraction features as are observed for semicrystalline cellulose type I (also referred to as native cellulose), which is corroborated by the characteristic peaks at $2\theta = 14.7°$, 16.8° and 22.7° corresponding to the 110, 110 and 200 crystallographic planes of monolithic cellulose type I, respectively (PDF files: 00-056-1717, 00-056-1718 and 00-056-1719).

The crystallinity index and crystallite size inferred from the XRD diffractograms for the unmodified cotton fibers were

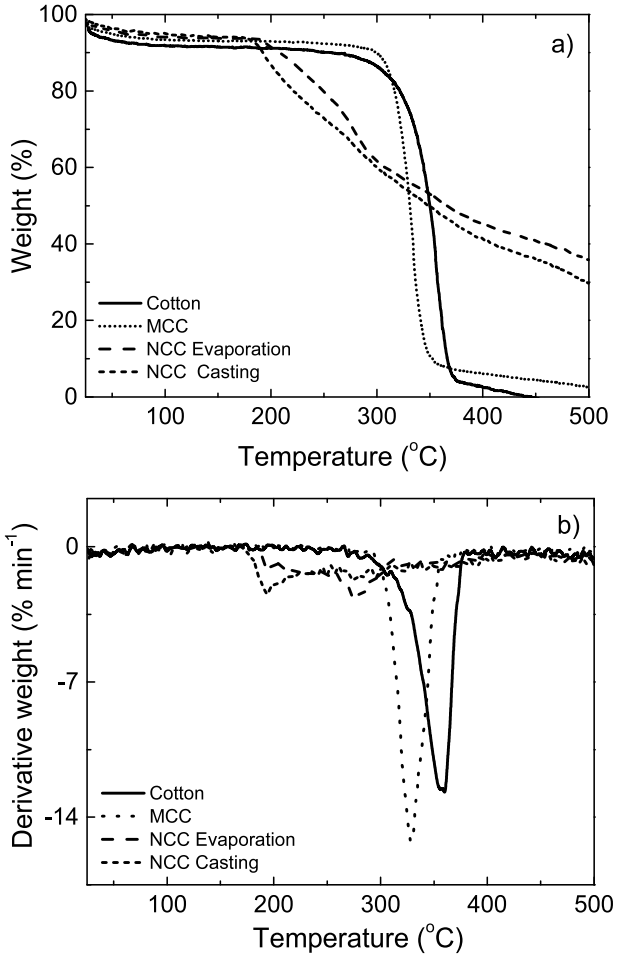

Figure 7. Thermal analysis of cotton fibers, microcrystalline cellulose particles and nanocrystalline cellulose membranes: (a) TGA and (b) DTG curves.

Table 2. Crystallinity index and crystallite size calculated from the x-ray diffractograms.

Sample	2θ (deg)	I_c (%)	D_{002} (nm)
Cotton	22.90	61	6.14
MCC	22.77	88	7.42
NCC E	22.83	81	7.29
NCC C	22.79	81	7.18

61% and 6.14 nm, respectively. The acid hydrolysis reaction for the production of microcrystalline cellulose improved the crystallinity index to 88% and the crystallite size to 7.42 nm. This may be due to the removal of impurities on the fibers or attributed directly to attaching nanocrystalline cellulose. For the nanocrystalline cellulose films, similar values have been obtained for the crystallite index as well as the crystallite size. A summary of the results obtained is presented in table 2. The values obtained are in accordance with reported values available in literature [40, 41].

The thermogravimetry results for the different materials under analysis are shown in figures 7(a) and (b) where we represent the residual mass as well as the derivative weight as a function of temperature, which permits the study of the thermal stability of nanocrystalline cellulose films.

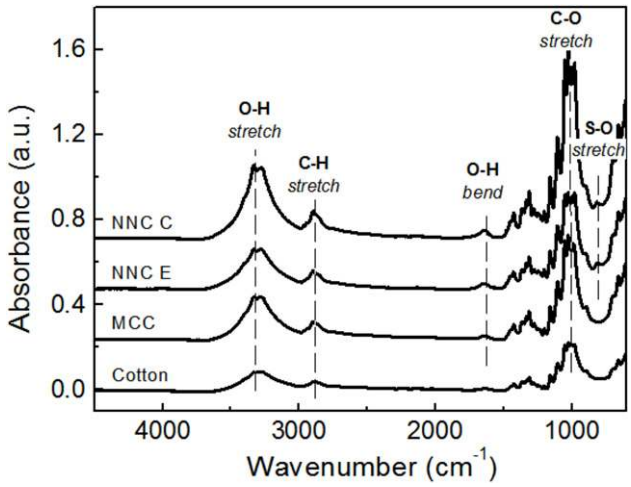

Figure 8. FTIR spectra of cotton fibers, microcrystalline cellulose particles and nanocrystalline cellulose membranes, as indicated inside the figure.

For the cotton fibers and the microcrystalline cellulose we observe a decomposition in the 280–380 °C region, while the nanocrystalline cellulose films decompose at significantly lower temperatures, between 170 and 310 °C, which is also consistent with the maximum degradation temperature shown in figure 7(b). This lowered temperature for the nanocrystalline cellulose films could be attributed to smaller fiber dimensions (190 nm) as compared to the original macroscopic fibers (see figure 4(b)), due to a higher surface area exposed to heat. It is also suggested that sulfate groups are expected to lower the degradation temperature due to the lower activation energy of decomposition from the surface sulfate groups. Similar thermal decomposition profiles were obtained by Morais *et al*for NCCs derived from raw cotton [37]. Regardless of the reduced thermal stability, the nanocrystalline cellulose films present much higher char residues of 33% on average, more than 16 times the finding for the original cotton fibers (∼2%). Increased char residues have been obtained from nanocrystalline cellulose from other origins, like bacteria cellulose as well as wood, and have been correlated with the dehydration reaction of the sulfate groups at lower temperatures, which are related to the smaller fiber dimensions resulting in lower thermal energy requirements.

FTIR spectra of the original cotton fibers, microcrystalline cellulose particles and nanocrystalline cellulose films are presented in figure 8. They show the same cellulose characteristic FTIR peaks, i.e. O–H, CH and C–O stretching vibrations at 3400 cm^{-1}, 2900 cm^{-1} and 1060 cm^{-1}, respectively, as does the cotton source used. The peak at 1640 cm^{-1} associated with the O–H bending vibration of absorbed water is more accentuated for the nanocrystalline cellulose films. The existence of peaks in the range of 1000–750 cm^{-1} can be assigned to S–O bond stretching due to the presence of sulfate groups in the NCC surface (see figure 8: the peak at 817 cm^{-1}). However the asymmetric and symmetric stretching of the S=O bond at 1350 and 1175 cm^{-1}, respectively, are not

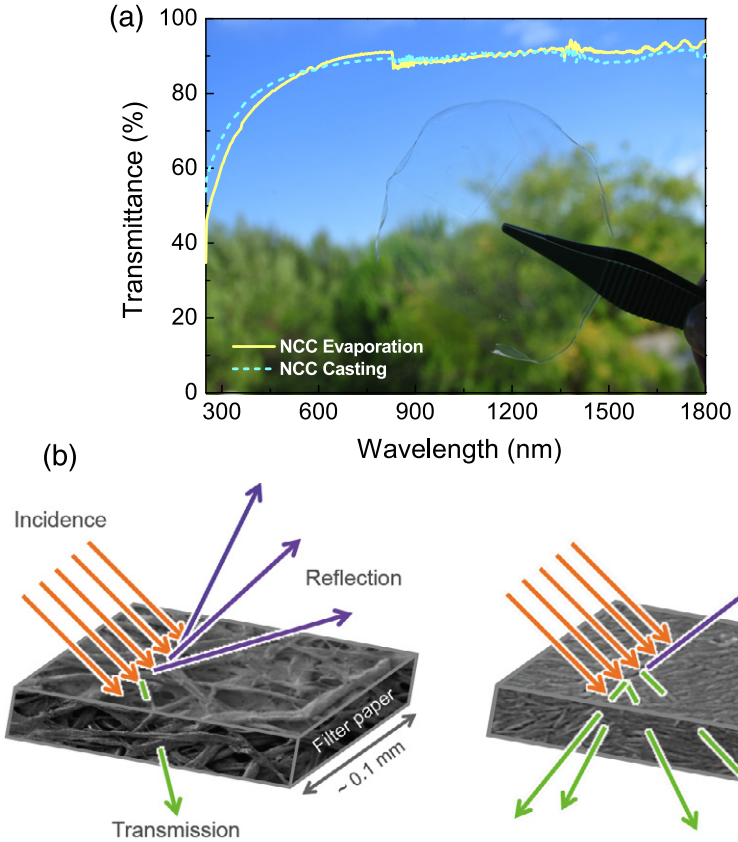

Figure 9. (a) Transmittance as a function of wavelength for the two NCC membranes. The graphic background shows a photograph of an NCC membrane prepared by solvent evaporation with a thickness of 30 μm; (b) schematic representation of a typical cellulose opaque paper (chromatography paper) and nanocellulose transparent paper. The average widths of the cellulose fibers and the nanocellulose fibers are 10 μm and 20 nm, respectively.

so noticeable since the cotton already presents several peaks around these regions [37, 42].

The NCCs are optically transparent, as can be seen in figure 9(a). The superior optical properties presented by these films are attributed to the densely packed nanofibers drastically reducing the voids between the fibers and avoiding light scattering (see the schematic representation in figure 9(b)) [43]. The two NCC membranes present similar optical properties over the entire wavelength range, presenting an average transmittance of 85% in the visible region of the spectrum, for a thickness of 30 μm.

3.2. Field effect transistors

Before testing the field effect transistors electrically we have measured the relative permittivity and loss tangent with respect to frequency for the two membranes under analysis, as is presented in figure 10. We observe an increase in the capacitance for low frequencies which is attributed to electrode polarization, that is, the interaction of the charged electrode surface with free charges in the paper, as happens for electric double-layer (EDL) capacitors [44]. The peak observed for tan δ indicates the relaxation frequency, that is, it separates the contribution of the bulk material itself from the contribution of the EDL. The latter extends then to the lowest frequency

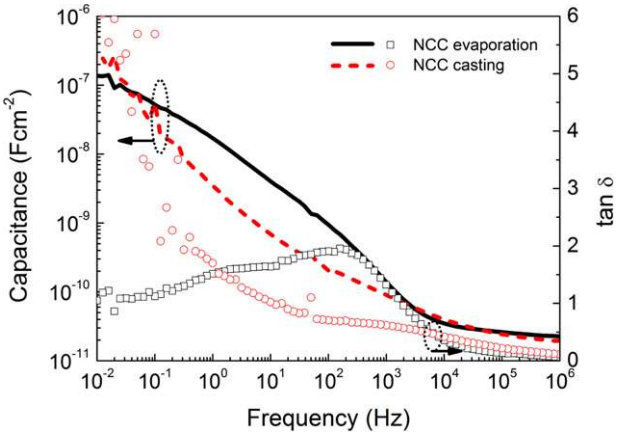

Figure 10. Capacitance and tan δ variation with frequency for both kinds of NCC membranes.

limit. This clearly indicates that the channel formation in the transistors will result from the presence of the EDL.

The strong increase in tan δ for the NCC casting sample means that it becomes leaky at low frequencies (the value is well above 1, that is, the dc conductivity of the NCC cannot be neglected), leading to a degradation of the nanocomposite.

Figure 11 shows the transfer and the output characteristics of two GIZO field effect transistors, with $W/L = 10.6$, in

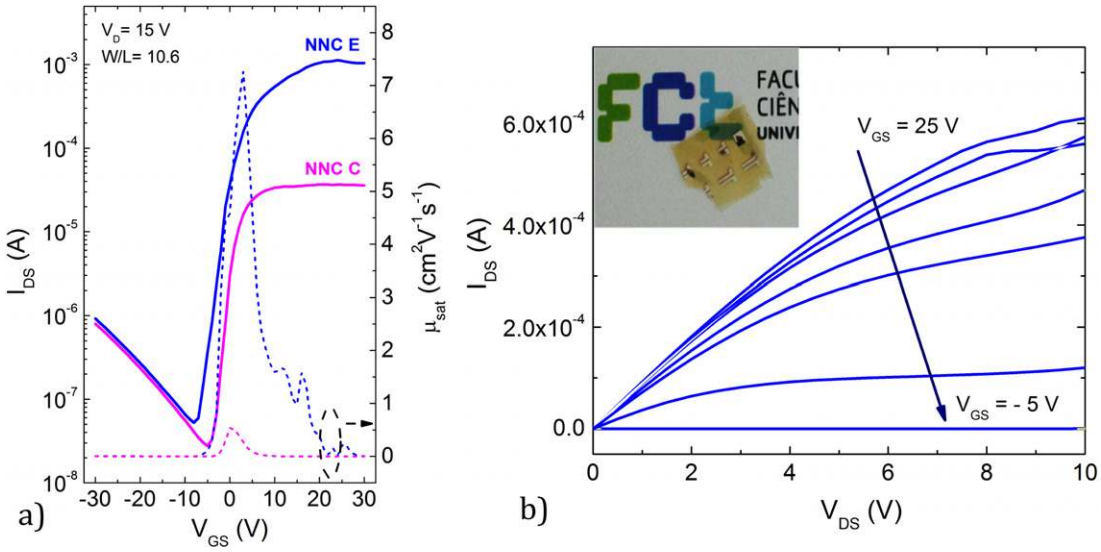

Figure 11. (a) I_{DS}–V_{GS} transfer characteristics obtained at $V_D = 15$ V (saturation region) for GIZO field effect transistors using two types of gate dielectric-based nanocrystalline cellulose; (b) output characteristics for the GIZO field effect transistor with an NCC membrane prepared by evaporation as the gate dielectric (the step for the gate voltage was 5 V, starting from −5 and going to 30 V). The inset shows an optical photograph of a fully processed FET.

Table 3. Comparison of the electrical properties of GIZO-based FETs with nanocrystalline cellulose based on different gate dielectrics.

Dielectric	μ_{sat} ($cm^2\ V^{-1}\ s^{-1}$)	V_{ON} (V)	I_{ON}/I_{OFF}	S (V/decade)
NCC evaporation	7.27	−8	2×10^5	2.11
NCC casting	0.54	−5	1×10^4	1.79
Reference cellulose paper [45]	16	−5	7.5×10^4	1.2

the saturation region ($V_D = 15$ V), using the two kinds of nanocrystalline cellulose films as the gate dielectric. The saturation mobility (μ_{sat}) and gate threshold voltage were calculated from the derivative and the x-axis intercept of the $\sqrt{I_D}(V_G)$ plot, respectively [20]. The subthreshold gate swing value (S) was obtained at the maximum slope of $dV_G/d(\log I_D)$. Table 3 presents a comparison of the electrical parameters of the two series of nanocrystalline cellulose-based GIZO FETs.

The electronic performances obtained for the devices do not differ significantly when the nanocrystalline cellulose fibers are used as the gate dielectric in comparison with the use of reference FETs using conventional cellulose paper [45]. The main differences observed for the devices using the two nanocrystalline cellulose films are related to the lower I_{ON} value, especially for nanocrystalline cellulose film produced by shear casting. This can be attributed to the higher surface roughness in comparison with that of the nanocrystalline cellulose film produced by evaporation, leading to a poor interface between the dielectric and the semiconductor material. Besides that, due to the lower thermal properties presented by the nanocrystalline film, especially that produced by casting, we start to have an electrical degradation at the interface of the aluminum (source/drain) which is responsible for the higher resistance, so limiting the drain current in the channel.

The output characteristics do not show a hard saturation behavior, which can be attributed to electrical contact effects. Besides that and since we are using shadow masks, the patterned semiconductor is not fully aligned with the source/drain regions which leads to a misalignment associated with the pinch-off region promoting possible pathways for the current, limiting the saturation regime.

4. Conclusions

We have produced high-performance hybrid flexible field effect transistors using nanocrystalline cellulose films produced from an anisotropic water gel by shear casting and from a diluted water suspension by casting and evaporation. These films were used (without any surface treatment) as the gate dielectric, and a semiconductor oxide (GIZO), deposited by r.f. magnetron sputtering at room temperature, as the channel layer. The transistors processed in this way have an enhancement of the n-type operation mode and exhibit a channel saturation mobility exceeding 7 $cm^2\ V^{-1}\ s^{-1}$, a drain–source current I_{ON}/I_{OFF} modulation ratio above 10^5 and a subthreshold gate voltage swing of about 2.11 V/decade.

The preliminary results obtained seem to surpass those for amorphous Si TFTs and rivals with the actual state of art for oxide-based thin film transistors produced on conventional paper [45], even the ones processed either on glass or on

crystalline silicon substrates, processed or annealed at high temperatures.

Transparent nanocrystalline cellulose films open up new perspectives for applications for cellulose devices. The compatibility of these devices with large-scale/large-area deposition techniques and low cost substrates marks this out as a promising approach for attaining high-performance disposable electronics like paper displays, smart labels, smart packaging, RFID and point-of-care systems for self-analysis in bioscience applications, among others.

We are watching the unfolding of one of the greatest opportunities for innovation in the forest products industry: the production and use of cellulose nanomaterials for a broad range of applications.

Work is under way in efforts to understand the operating mechanism of the device, in order to improve its stability over time.

Acknowledgments

This work was financed by the European Commission under projects INVISIBLE (FP7 ERC AdG No. 228144), ORAMA CP-IP 246334-2, and APPLE (FP7-NMP-2010-SME/262782-2), and the Portuguese Science Foundation (FCT-MEC) through the Projects PEst-C/CTM/LA0025/2013-14, EXCL/CTM-NAN/0201/2012, PTDC/CTM/103465/2008, PTDC/CTM-POL/1484/2012 and grant SFRH/BPD/78430/2011 to S N Fernandes.

The authors would like to thank their colleagues Daniela Nunes, Sónia Pereira and Ana Pimentel, for the SEM, XRD and TG measurements, respectively.

References

[1] Tobjork D and Osterbacka R 2011 Paper electronics *Adv. Mater.* **23** 1935–61

[2] Fortunato E, Correia N, Barquinha P, Pereira L, Goncalves G and Martins R 2008 High-performance flexible hybrid field-effect transistors based on cellulose fiber paper *IEEE Electron Device Lett.* **29** 988–90

[3] Martins R, Barquinha P, Pereira L, Correia N, Goncalves G, Ferreira I and Fortunato E 2008 Write–erase and read paper memory transistor *Appl. Phys. Lett.* **93** 203501

[4] Martins R, Nathan A, Barros R, Pereira L, Barquinha P, Correia N, Costa R, Ahnood A, Ferreira I and Fortunato E 2011 Complementary metal oxide semiconductor technology with and on paper *Adv. Mater.* **23** 4491

[5] Martins R F P, Ahnood A, Correia N, Pereira L M N P, Barros R, Barquinha P M C B, Costa R, Ferreira I M M, Nathan A and Fortunato E E M C 2013 Recyclable, flexible, low-power oxide electronics *Adv. Funct. Mater.* **23** 2153–61

[6] Martins R, Ferreira I and Fortunato E 2011 Electronics with and on paper *Phys. Status Solidi—Rapid Res. Lett.* **5** 332–5

[7] Martins R *et al* 2011 Away from silicon era: the paper electronics *Oxide-Based Materials and Devices II* vol 7940, ed F H Teherani, D C Look and D J Rogers 79400P

[8] Geng Y, Almeida P L, Fernandes S N, Cheng C, Palffy-Muhoray P and Godinho M H 2013 A cellulose liquid crystal motor: a steam engine of the second kind *Sci. Rep.* **3** 1028

[9] Fernandes S N, Geng Y, Vignolini S, Glover B J, Trindade A C, Canejo J P, Almeida P L, Brogueira P and Godinho M H 2013 Structural color and iridescence in transparent sheared cellulosic films *Macromol. Chem. Phys.* **214** 25–32

[10] Dong X M, Kimura T, Revol J-F and Gray D G 1996 Effects of ionic strength on the isotropic–chiral nematic phase transition of suspensions of cellulose crystallites *Langmuir* **12** 2076–82

[11] Cranston E D and Gray D G 2006 Morphological and optical characterization of polyelectrolyte multilayers incorporating nanocrystalline cellulose *Biomacromolecules* **7** 2522–30

[12] Habibi Y, Lucia L A and Rojas O J 2010 Cellulose nanocrystals: chemistry, self-assembly, and applications *Chem. Rev.* **110** 3479–500

[13] Henriksson M, Berglund L A, Isaksson P, Lindstrom T and Nishino T 2008 Cellulose nanopaper structures of high toughness *Biomacromolecules* **9** 1579–85

[14] Petersen N and Gatenholm P 2011 Bacterial cellulose-based materials and medical devices: current state and perspectives *Appl. Microbiol. Biotechnol.* **91** 1277–86

[15] Peng B L, Dhar N, Liu H L and Tam K C 2011 Chemistry and applications of nanocrystalline cellulose and its derivatives: a nanotechnology perspective *Can. J. Chem. Eng.* **89** 1191–206

[16] Klemm D, Kramer F, Moritz S, Lindstrom T, Ankerfors M, Gray D and Dorris A 2011 Nanocelluloses: a new family of nature-based materials *Angew. Chem. Int. Edn Engl.* **50** 5438–66

[17] Dufresne A 2012 *Nano-Cellulose, From Nature to High Performance Tailored Materials* (Berlin: de Gruyter & Co.)

[18] Lee S Y, Mohan D J, Kang I A, Doh G H, Lee S and Han S O 2009 Nanocellulose reinforced PVA composite films: effects of acid treatment and filler loading *Fibers Polym.* **10** 77–82

[19] Aulin C, Salazar-Alvarez G and Lindstrom T 2012 High strength, flexible and transparent nanofibrillated cellulose–nanoclay biohybrid films with tunable oxygen and water vapor permeability *Nanoscale* **4** 6622–8

[20] Huang J, Zhu H L, Chen Y C, Preston C, Rohrbach K, Cumings J and Hu L B 2013 Highly transparent and flexible nanopaper transistors *ACS Nano* **7** 2106–13

[21] Hsieh Y-L 2007 Chemical structure and properties of the cotton *Cotton: Science and Technology* ed S Gordon and Y-L Hsieh (Cambridge: Woodhead Publishing) pp 3–34

[22] Hsieh Y-L 2013 Cellulose nanocrystals and self-assembled nanostructures from cotton, rice straw and grape skin: a source perspective *J. Mater. Sci.* **48** 7837–46

[23] Abidi N, Hequet E and Cabrales L 2010 Changes in sugar composition and cellulose content during the secondary cell wall biogenesis in cotton fibers *Cellulose* **17** 153–60

[24] Fortunato E, Barquinha P and Martins R 2012 Oxide semiconductor thin-film transistors: a review of recent advances *Adv. Mater.* **24** 2945–86

[25] Barquinha P, Pereira L, Goncalves G, Martins R and Fortunato E 2009 Toward high-performance amorphous GIZO TFTs *J. Electrochem. Soc.* **156** H161–8

[26] Barquinha P, Vila A M, Goncalves G, Martins R, Morante J R, Fortunato E and Pereira L 2008 Gallium–indium–zinc-oxide-based thin-film transistors: influence of the source/drain material *IEEE Trans. Electron Devices* **55** 954–60

[27] Barquinha P, Pereira L, Goncalves G, Martins R and Fortunato E 2008 The effect of deposition conditions and

annealing on the performance of high-mobility GIZO TFTs *Electrochem. Solid State Lett.* **11** H248–51
[28] Nada A-A M A, El-Kady M Y, El-Sayed E S A and Amine F M 2009 Preparation and characterization of microcrystalline cellulose (MCC) *BioResources* **4** 1359–71
[29] Stephens C H, Whitmore P M, Morris H R and Bier M E 2008 Hydrolysis of the amorphous cellulose in cotton-based paper *Biomacromolecules* **9** 1093–9
[30] Chauhan Y P, Sapkal R S, Sapkal V S and Zamre G S 2009 Microcrystalline cellulose from cotton rags (waste from garment and hosiery industries) *Int. J. Chem. Sci.* **7** 681–8
[31] Revol J-F, Bradford H, Giasson J, Marchessault R H and Gray D G 1992 Helicoidal self-ordering of cellulose microfibrils of cellulose microfibrils in aqueous suspension *Int. J. Biol. Macromol.* **14** 170–2
[32] Orts W J, Shey J, Imam S H, Glenn G M, Guttman M E and Revol J-F 2005 Application of cellulose microfibrils in polymer nanocomposites *J. Polym. Environ.* **13** 301–6
[33] Segal J J C L, Martin A E Jr and Conrad C M 1959 An empirical method for estimating the degree of crystallinity of native cellulose using the x-ray diffractometer *Text. Res. J.* **29** 786–94
[34] Klug H P A and Leroy E 1974 *X-Ray Diffraction Procedures: For Polycrystalline and Amorphous Materials* 2nd edn (New York: Wiley)
[35] Barquinha P, Goncalves G, Pereira L, Martins R and Fortunato E 2007 Effect of annealing temperature on the properties of IZO films and IZO based transparent TFTs *Thin Solid Films* **515** 8450–4
[36] Lima M M D and Borsali R 2004 Rodlike cellulose microcrystals: structure, properties, and applications *Macromol. Rapid Commun.* **25** 771–87
[37] Morais J P S, Rosa M de F, de Souza Filho M de sá M, Nascimento L D, do Nascimento D M and Cassales A R 2013 Extraction and characterization of nanocellulose structures from raw cotton linter *Carbohydr. Polym.* **91** 229–35
[38] Elazzouzi-Hafraoui S, Nishiyama Y, Putaux J-L, Heux L, Dubreuil F and Rochas C 2008 The shape and size distribution of crystalline nanoparticles prepared by acid hydrolysis of native cellulose *Biomacromolecules* **9** 57–65
[39] Majoinen J, Kontturi E, Ikkala O and Gray D G 2012 SEM imaging of chiral nematic films cast from cellulose nanocrystal suspensions *Cellulose* **19** 1599–605
[40] Morais J P S, Rosa M D, de Souza M D M, Nascimento L D, do Nascimento D M and Cassales A R 2013 Extraction and characterization of nanocellulose structures from raw cotton linter *Carbohydr. Polym.* **91** 229–35
[41] Teixeira E D, Correa A C, Manzoli A, Leite F L, de Oliveira C R and Mattoso L H C 2010 Cellulose nanofibers from white and naturally colored cotton fibers *Cellulose* **17** 595–606
[42] Abidi N, Hequet E, Cabrales L, Gannaway J, Wilkins T and Wells L W 2008 Evaluating cell wall structure and composition of developing cotton fibers using Fourier transform infrared spectroscopy and thermogravimetric analysis *J. Appl. Polym. Sci.* **107** 476–86
[43] Nogi M, Iwamoto S, Nakagaito A N and Yano H 2009 Optically transparent nanofiber paper *Adv. Mater.* **21** 1595
[44] Ma L P and Yang Y 2005 Solid-state supercapacitors for electronic device applications *Appl. Phys. Lett.* **87** 123503
[45] Pereira L 2014 The influence of fibril composition and dimension on the performance of paper gated oxide transistors *Nanotechnology* **25** 094007